Available online at www.sciencedirect.com
ScienceDirect
Mathematics and Computers in Simulation 175 (2020) 96–107
MATHEMATICS AND COMPUTERS IN SIMULATION
www.elsevier.com/locate/matcom

Orginal articles

The terminal-velocity assumption in simulations of long-range ember transport

C.M. Thomas[a,c,*], J.J. Sharples[b,c], J.P. Evans[a]

[a] *Climate Change Research Centre, University of New South Wales Australia, Sydney 2052, Australia*
[b] *School of Science, University of New South Wales, Canberra, ACT 2610, Australia*
[c] *Bushfire and Natural Hazards Cooperative Research Centre, Level 1, 340 Albert St, East Melbourne 3002, Australia*

Received 17 May 2018; received in revised form 10 August 2019; accepted 12 August 2019
Available online 20 August 2019

Abstract

Ember transport and the subsequent development of spot fires is a significant mode of wildfire spread, particularly in extreme conditions. An important simplifying assumption made in early research into ember transport is the *terminal-velocity assumption*, in which embers are assumed to always fly at their terminal velocity relative to the wind field. With increases in computational power, it is now possible to directly simulate the atmospheric conditions resulting from wildfires and such simulations can resolve the larger of the turbulent processes involved. Because of the time-scales at which these processes occur, the terminal-velocity assumption may not be justified when modelling ember transport using these simulations. In this study we use a large eddy simulation of a turbulent plume to examine the validity of the terminal-velocity assumption when modelling the long-range transport of non-combusting embers. The results indicate that the use of the terminal-velocity assumption significantly overestimates the density of ember landings at long range, particularly for embers with higher terminal fall speeds.

Keywords: Ember transport; Firebrands; Spot fires; Terminal-velocity assumption

1. Introduction

1.1. Early work and the terminal velocity assumption

Early workers researching ember transport used a combination of empirical and analytical techniques with suitable simplifying assumptions. Using the quadratic drag law for high Reynolds-number flow [2], Tarifa and del Notario [13] wrote down the equations of motion of an ember moving with velocity $\mathbf{u}$ in a wind field with velocity $\mathbf{w}$ as

$$\frac{\mathrm{d}\mathbf{u}}{\mathrm{d}t} = \frac{C_\mathrm{d}\rho A}{2m}|\mathbf{w}-\mathbf{u}|(\mathbf{w}-\mathbf{u}) - g\mathbf{k} \tag{1}$$

* Corresponding author at: Climate Change Research Centre, University of New South Wales Australia, Sydney, 2052, Australia
E-mail address: christopherthomas@cmt.id.au (C.M. Thomas).

https://doi.org/10.1016/j.matcom.2019.08.008

where C_d is the ember's drag coefficient, ρ is the atmospheric density, m is the mass of the ember, A its projected area in the direction of the relative wind velocity $\mathbf{w}-\mathbf{u}$, and $\mathbf{k}$ is the unit vector in the z-direction; see also [14]. In deriving Eq. (1) it was assumed that the drag force acts through the centre of mass of the particle and that the lift force, i.e. the aerodynamic force perpendicular to the direction of the relative wind, is zero. Each of the quantities in the expression $\alpha \equiv C_d \rho A/2m$ may vary as the particle moves within the atmosphere, changes orientation with respect to the relative wind $\mathbf{w}-\mathbf{u}$, and loses mass and changes geometry through combustion. However, under the assumption that α and $\mathbf{w}$ are constant, and choosing the x-direction parallel to $\mathbf{w}-\mathbf{u}$, Tarifa and del Notario [13] wrote Eq. (1) as a system of two equations and obtained its analytical solution. They showed that for values of α typical of an ember the solution rapidly (i.e. within a few seconds) approaches the asymptotic solution

$$\mathbf{u}_\infty = \mathbf{w} - \sqrt{\frac{2mg}{C_d \rho A}}\,\mathbf{k} \tag{2}$$

where $u_\infty \equiv \sqrt{2mg/C_d\rho A}$ is the terminal (fall) speed of the ember. Since changes in ember characteristics due to combustion occur at longer time scales than a few seconds, Tarifa and del Notario [13] concluded that for constant or slowly-varying wind conditions there was little error in assuming that embers always travel at their terminal velocity $\mathbf{u}_\infty$. This so-called *terminal-velocity assumption* greatly simplifies analytical work and was used extensively by early researchers, either because of the lack of high-speed computing resources or in order to produce simple models of potential spotting distance for use in the field (e.g. [1,14]).

1.2. Aerodynamic lift and rotational motion

Eq. (1) is not the most general equation of motion that can be applied: it neglects the effects of rotation and aerodynamic lift which occur for non-spherical embers, as well as some subtle effects related to unsteady flow [9]. In very small-scale wind-tunnel experiments, Wadhwani et al. [22] found that simulations based on Eq. (1) could reproduce empirical landing distributions of cubiform (essentially spherical) particles but not those of cylindrical particles. Some authors have incorporated aerodynamic lift into the equations of motion, but with simplifications such as assuming that the lift force has no horizontal component, or that the ember maintains a constant angle of attack with respect to the relative wind (e.g. [6,10]). However a complete treatment of lift and rotation requires a set of equations that describe the translational and rotational motion of an ember with 6 degrees of freedom (DoF). Richards et al. [9] used a wind tunnel to measure, under conditions of steady flow, the normal forces and turning moments on fixed plates and rods, and used these coefficients in a set of 6-DoF equations to validate qualitatively the predicted trajectories of plates and rods against those observed in wind-tunnel experiments. Using drop-fall and wind-tunnel experiments, and simulations with a large eddy model (LEM), Tohidi and Kaye [19,20,21] validated statistically the use of these steady coefficients. Himoto and Tanaka [5] used 6-DoF equations of motion and a LEM to simulate the transport of disc-shaped embers in a turbulent boundary layer into which a static heat source had been introduced, using normal forces and turning moments obtained experimentally by Tachikawa and Fukuyama [12]. These were small-scale simulations on a domain of $124 \times 50 \times 50$ cells ($x \times y \times z$). Oliveira et al. [8] used a 6-DoF model for cylindrical embers, with semi-empirical expressions for the drag coefficients and turning moments, and validated this model qualitatively using drop tests in still air. In numerical simulations of the fall of a cylindrical ember from 200 m in a non-turbulent wind field with a logarithmic profile, they found that travel distances depended significantly on the initial orientation of the ember [8], underlining the point that rotational motion has an effect on ember trajectories.

1.3. This study

The studies discussed in Section 1.2 were all at small scales whereas this paper is concerned with the simulation of long-range ember transport in turbulent plumes. The results of [8,19,21,22] indicate that Eq. (1) (and therefore Eq. (2)) is not sufficient to model the short-range transport of non-spherical embers. However it is not known how these results scale to long-range ember transport. For example, while the results in [8] show that initial orientation has a significant effect on the modelled travel distance of cylindrical embers falling 200 m in a horizontal wind field, it is not clear how important the initial orientation will be when calculating the landing distribution of

embers travelling more than 10 km in a turbulent plume. The use of a full 6-DoF model for simulations of long-range transport is likely to be computationally demanding and the appropriate level of model complexity for such simulations is not obvious. In this paper we make steps in this direction. We do not consider rotational motion, but focus on the differences between Eqs. (1) and (2).

It is now possible to numerically model at landscape scales the atmospheric conditions associated with wildfires and these models can resolve the larger turbulent processes involved. Thurston et al. [17] made what may be the first numerical study of long-range ember transport, using a LEM to simulate a turbulent plume and modelling the transport of embers over distances of up to 20 km. They made a strong form of the terminal-velocity assumption, using Eq. (2) with a constant terminal-fall speed u_∞. However the wind fields generated in such a model can change at time scales shorter than the time it takes for the solution of Eq. (1) to relax to Eq. (2), and this calls into question the validity of the terminal-velocity assumption when modelling ember transport in this context. Previously Koo et al. [6] found that, in numerical modelling of ember transport from grass fires, the use of the terminal-velocity assumption significantly underestimated the distance that embers were transported compared with simulations which accounted for the momentum of the embers (as does Eq. (1)). This modelling was done at small to medium scales (the computational domain was 640 × 320 × 615 m) and they attributed their results to the fact that due to their momentum embers 'can fly faster than their immediate-surrounding winds' [6]. While this is true, for the same reason they can also fly more slowly, or in the opposite direction. It is not clear whether the use of the terminal-velocity assumption results in a systematic bias in travel distances when modelling long-range ember transport.

In the current study we perform large-scale LEM simulations of a turbulent plume resulting from a static heat source in a turbulent boundary layer, similar to those of Thurston et al. [17]. We then carry out ember transport calculations with and without making the terminal-velocity assumption and compare the results. We do not examine individual ember trajectories but focus on the density of ember landings, both because this allows us to treat a large number of embers ($\sim 3 \times 10^6$), and because this density is an important determinant of the likelihood of spot-fire ignition. It is not our intention to produce realistic ember-landing distributions; for one thing our simulations do not include the effects of in-flight combustion which will have a significant effect on ember trajectories. Rather, we are trying to assess whether the terminal-velocity assumption is justified when modelling long-range ember transport in turbulent wind fields.

This paper is based on work presented at the 22nd International Congress on Modelling and Simulation [16]. In the current study we have extended the simulations to include embers with a 3 m s^{-1} terminal fall speed, randomised the initial positions of the simulated embers, and made an analysis of the accuracy and stability of the numerical scheme. We have also provided more details on the structure of the simulated turbulent plume, and on the historical context in which the work lies.

2. The model

2.1. Large eddy simulation of turbulent boundary layer

In the first stage of the modelling the Weather Research and Forecasting (WRF) atmospherical model [11] was used in LEM mode to spin up a turbulent boundary layer in a domain of 40 × 16 × 12 km ($x \times y \times z$). The horizontal resolution of the computational grid was 50 m, and the vertical coordinate system consisted of 256 levels spaced at approximately 10 m at the surface, increasing to approximately 50 m at the model top. In practice the vertical spatial resolution may vary slightly during a simulation because of the pressure-based vertical coordinate system used by the WRF model [11].

Periodic boundary conditions were used for the lateral (x-y) boundaries so that developing turbulent eddies are recycled as they are advected across the downwind boundary. This allows the simulated development of a shear-driven turbulent boundary layer without necessitating a prohibitively large computational domain. A 1000 m deep Rayleigh-damping layer was used at the top of the model domain. Turbulence was parametrised using a 1.5-order turbulent kinetic energy (TKE) scheme.

The model was initialised with a 3-km-deep dry-adiabatic layer with an almost constant potential temperature of $\theta = 300$ K. Small random perturbations of θ were introduced in this layer to stimulate the development of turbulence. This dry-adiabatic layer was topped by a stable layer with a lapse rate of 3 K per km. The initial wind profile consisted of a constant value of $w_x = 15$ m s^{-1} over the entire model depth, with $w_y = w_z = 0$.

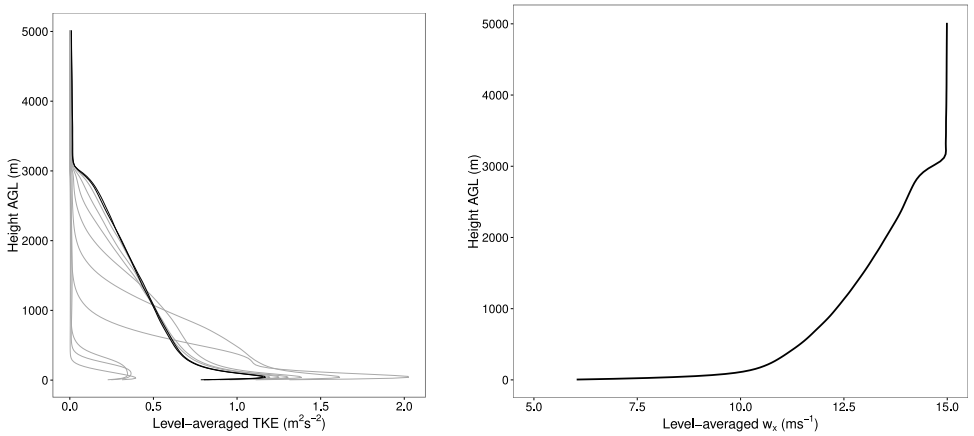

(a) Level-averaged TKE (b) Level-averaged w_x

Fig. 1. (a) Evolution of total (subgrid scale + resolved) turbulence kinetic energy (TKE) during the spin-up phase of the simulation. The grey lines show the level-averaged TKE hourly for the first 9 h. The black lines (almost identical) show the level-averaged TKE at $t =$ 10:00 and $t =$ 11:00 h. (b) Level-averaged x-component of wind field, w_x, at $t =$ 10:00 h, immediately prior to application of sensible heat flux.

The model was run for 10 h of model time after which a turbulent boundary layer had developed; the vertical profile of TKE had stabilised (Fig. 1(a)), and the level-averaged value of w_x had assumed the vertical profile seen in Fig. 1(b), consistent with a shear-driven turbulent boundary layer [7].

2.2. Development of simulated plume

Once a turbulent boundary layer had developed, a plume was simulated by introducing a heat source at the lower boundary of the model domain. This was done by modifying the WRF-Fire code [3] which, during a coupled atmosphere-fire simulation, inputs sensible and latent heat fluxes to the WRF atmospheric model. In the full WRF-Fire model these fluxes are derived from a semi-empirical fire-spread submodel; our modified code simulates a static heat flux. Following Thurston et al. [18] (see also [17]) we used a circular surface sensible-heat-flux anomaly, with intensity 10^5 W m^{-2} and radius 250 m, located 2 km inside the upwind boundary of the computational domain. In common with Thurston et al. [17], no latent heat (i.e. moisture) flux was assumed. While the inclusion of such a flux may or may not alter the modelled ember landing distributions, we would not expect it to alter the conclusions of this paper which is concerned with differences in ember landing distributions under various transport assumptions. To allow the plume to develop and stabilise the simulation was continued for 1 h of model time. The simulation was then continued for another hour during which data were collected at 5-s intervals; it is these data that were used to compute ember trajectories. Fig. 2 shows cross sections of the turbulent wind field within the plume at the beginning of this period. The structure of the plume is consistent with that simulated by Thurston et al. [17] (their Fig. 1). The leading edge exhibits a series of thermals which rise above the main part of the plume (Fig. 2(a)), some of which extend above the mixed layer which ends at 3 km. Vertically-oriented vortical structures are evident, for example at coordinates (8, 8.5) in Fig. 2(b), and (10.5, 8.5) in Fig. 2(c).

2.3. Ember trajectory computations

2.3.1. Preliminaries

In their work, Thurston et al. [17] assumed ember velocities of the form

$$\mathbf{u} = \mathbf{w} - u_\infty \mathbf{k} \tag{CTVA}$$

with a constant value of u_∞. We will refer to Eq. (CTVA) as the *constant terminal-velocity assumption*. This is a rather strong form of the terminal-velocity assumption because according to Eq. (2) the terminal velocity of an

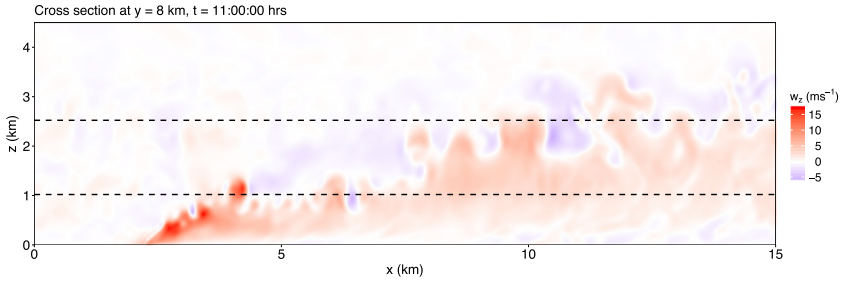

(a) Vertical cross section at $y = 8$ km.

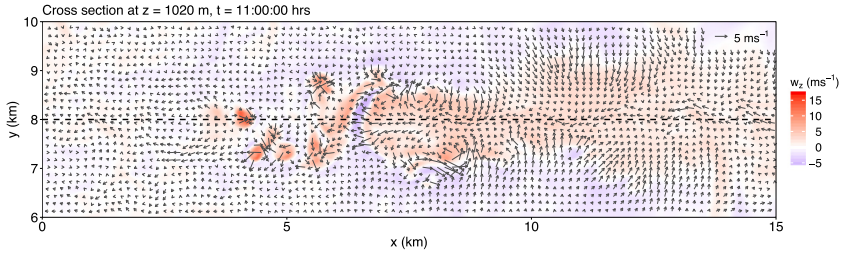

(b) Horizontal cross section at $z = 1.020$ km.

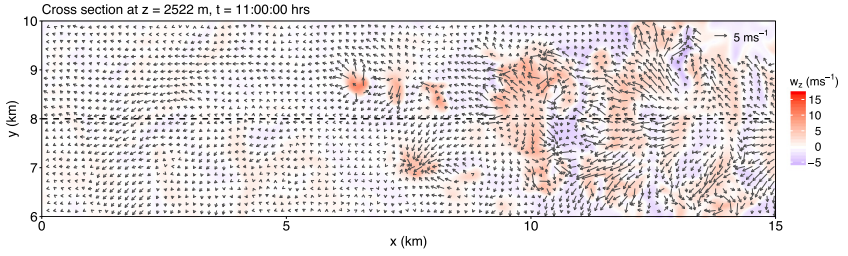

(c) Horizontal cross section at $z = 2.522$ km.

Fig. 2. Vertical and horizontal cross sections through the plume at $t = 11{:}00{:}00$ h, the time at which ember release begins. Vertical velocity is indicated by the colour scale. The vectors represent the horizontal velocity perturbations from the level-averaged values of Fig. 1(b). The locations of the cross sections are indicated by dashed lines.

ember depends on, among other things, the atmospheric density ρ. In this study we interpret the constant u_∞ in Eq. (CTVA) as the terminal fall speed of an ember at some reference atmospheric density ρ_0, so that

$$u_\infty = \sqrt{\frac{2mg}{C_\mathrm{d}\rho_0 A}}. \tag{3}$$

One might think of ρ_0 as the atmospheric density at the location of the experiments used to determine u_∞, and in this study we use $\rho_0 = 1.16$, the approximate atmospheric density at sea level. This is a reasonable but arbitrary choice; changes in the value of ρ_0 are equivalent to a scaling of the value of u_∞. Using Eq. (3) we can rewrite Eq. (1) as

$$\frac{\mathrm{d}\mathbf{u}}{\mathrm{d}t} = g\frac{\rho}{\rho_0}\frac{1}{{u_\infty}^2}|\mathbf{w}-\mathbf{u}|(\mathbf{w}-\mathbf{u}) - g\mathbf{k}. \tag{NTVA}$$

In this case no terminal velocity assumption is made. The differences between motion under Eqs. (CTVA) and (NTVA) are twofold: Eq. (NTVA) takes into account both the momentum of the embers and changes in ρ. The term ρ/ρ_0 in Eq. (NTVA) can be significantly different from unity both at higher altitudes and within the plume and it is likely that this will be an important factor contributing to any differences in ember motion under Eqs. (CTVA) and

(NTVA). An intermediate formulation which isolates this effect can be found by substituting Eq. (3) into Eq. (2) giving

$$\mathbf{u}_\infty = \mathbf{w} - \sqrt{\frac{\rho_0}{\rho}} u_\infty \mathbf{k}. \tag{VTVA}$$

This is the asymptotic solution of Eq. (NTVA) and we will refer to it as the *variable terminal-velocity assumption*.

The terminal fall speed u_∞ of the ember at the reference atmospheric density ρ_0 is the only explicit ember characteristic appearing in each of Eqs. (CTVA), (VTVA), and (NTVA). This makes it convenient to compare motion under these three equations since we need only specify a set of embers with initial positions $\mathbf{x}_0$ and terminal fall speeds u_∞ and apply each of Eqs. (CTVA), (VTVA), and (NTVA) to compute the trajectories of the embers in that set.

For non-spherical embers the quantities C_d and A in Eq. (3) depend on the direction of the relative wind velocity $\mathbf{w}-\mathbf{u}$. It is implicit in our formulation that these quantities remain constant during ember transport. This amounts to assuming that the ember always has the same orientation with respect to $\mathbf{w}-\mathbf{u}$, or that it adopts such an orientation over time scales much smaller than those over which $\mathbf{w}-\mathbf{u}$ changes. This assumption is similar in nature to the terminal-velocity assumption. The investigation of its validity for long-range ember transport is beyond the scope of this paper, however we note that it is supported to some extent by the studies of Ellis [4] and Tarifa et al. [15]; in drop tests embers either assumed an orientation of maximum drag, or tumbled but fell at a speed as if they had assumed such an orientation (but see the discussion in Section 1.2). Some numerical studies, including those of Himoto and Tanaka [5] and Oliveira et al. [8], include the rotational terms in the equations of motion.

2.3.2. Ember initialisation

In our modelling embers were released every 5 s for the first 30 min of the ember transport phase of the simulations. Embers were initialised at heights between 5 and 50 m, at locations where $w_z > 5\ \mathrm{m\,s^{-1}}$. Within these constraints the initial positions of embers were chosen randomly with an average separation of 5 m. These parameters are somewhat arbitrary however it should be remembered that the purpose of the current study is not to simulate realistic ember landing distributions, but to compare the differences in simulated ember landing distributions using three different ember transport assumptions. That being said, the range of release heights (5 to 50 m) seems reasonable having regard to the vertical grid resolution near the surface ($\sim$ 10 m) and the height of tall eucalypt forests. The requirement of a minimum vertical wind velocity of $5\ \mathrm{m\,s^{-1}}$ for ember launch also seems reasonable given the range of terminal velocities considered (3 to $8\ \mathrm{m\,s^{-1}}$). The parameter controlling average separation (set at 5 m) does not represent a known empirical fact or reasonable estimate, but was used to control the number of embers released in the numerical experiments; with these settings 3,280,660 embers were released in the first 30 min of the simulation, and tests showed that increasing the number of embers by reducing the average separation did not substantially alter the results. Because the initial positions are randomised it was not necessary to also randomise ember release times: if $\{t_n\}$ is the sequence of regular release times then, conceptually, the position of an ember released at a random location and time can be integrated forward or backward in time to another essentially random location at the nearest regular release time t_i. Consequently one can view the embers as in essence being released at random times throughout each 5-s period.

Embers were assigned terminal fall speeds of $u_\infty = 3$, 6, and $8\ \mathrm{m\,s^{-1}}$. These values are consistent with those from previous experimental and numerical studies: Ellis [4] measured terminal velocities in the range of 2.5 to $8\ \mathrm{m\,s^{-1}}$ for samples of eucalyptus bark, and Thurston et al. [17] modelled ember transport for $u_\infty = 5, 6, 7, 8$ and $9\ \mathrm{m\,s^{-1}}$. The same set of ember initial locations and starting times was used for each choice of u_∞.

Fig. 3 depicts embers in flight, modelled using Eq. (NTVA) with $u_\infty = 6\ \mathrm{m\,s^{-1}}$.

2.3.3. Numerical methods

The standard Runge–Kutta explicit second-order scheme (RK2) was used to compute trajectories under Eqs. (CTVA), (VTVA) and (NTVA). Thus for Eq. (VTVA), if $\mathbf{x}_{t_0}$ is the estimate of the position of an ember at time t_0, we first compute a temporary estimate at time $t_0 + \delta t/2$,

$$\mathbf{x}^* = \mathbf{x}_{t_0} + \left(\mathbf{w}(\mathbf{x}_{\mathbf{t_0}}, t_0) - \sqrt{\frac{\rho_0}{\rho(\mathbf{x}_{t_0}, t_0)}} u_\infty \mathbf{k} \right) \frac{\delta t}{2},$$

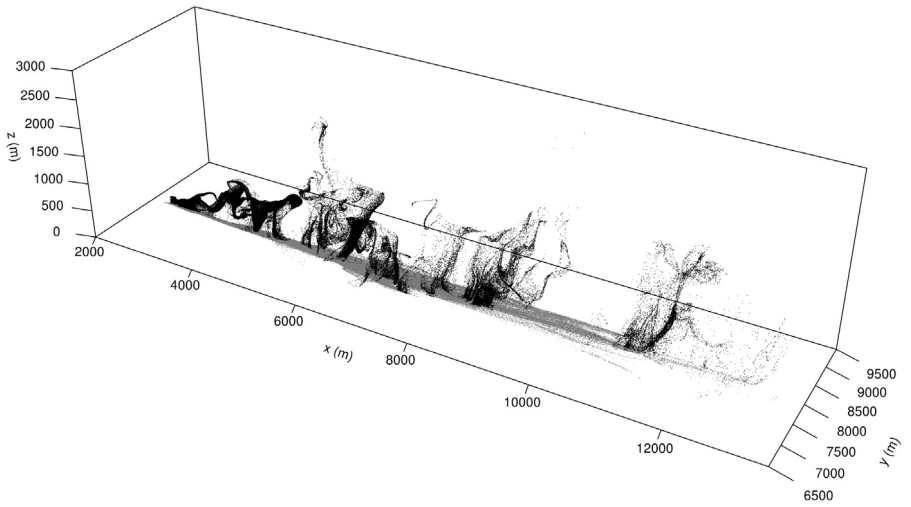

Fig. 3. Modelled embers in flight (black points), and after landing (grey points), 15 min into the ember transport phase of the modelling. In this case trajectories were computed using Eq. (NTVA) with $u_\infty = 6\ \mathrm{m\,s^{-1}}$. Only part of the computational domain is shown.

and then estimate $\mathbf{x}$ at time $t_0 + \delta t$ as

$$\mathbf{x}_{t_0+\delta t} = \mathbf{x}_{t_0} + \left(\mathbf{w}(\mathbf{x}^*, t_0 + \delta t/2) - \sqrt{\frac{\rho_0}{\rho(\mathbf{x}^*, t_0 + \delta t/2)}} u_\infty \mathbf{k} \right) \delta t.$$

Here, $\mathbf{w}(\mathbf{x}, t)$ and $\rho(\mathbf{x}, t)$ are interpolated linearly in time and space from the LEM output (Section 2.2). The method for Eq. (CTVA) is the same but with $\rho_0/\rho \equiv 1$. Eq. (NTVA), which is of second order, was converted to a first-order system in the usual way:

$$\frac{\mathrm{d}\mathbf{x}}{\mathrm{d}t} = \mathbf{u}$$
$$\frac{\mathrm{d}\mathbf{u}}{\mathrm{d}t} = \mathbf{a}(\mathbf{u}, \mathbf{x}, t)$$

where

$$\mathbf{a}(\mathbf{u}, \mathbf{x}, t) = g \frac{\rho(\mathbf{x}, t)}{\rho_0} \frac{1}{{u_\infty}^2} |\mathbf{w}(\mathbf{x}, t) - \mathbf{u}| (\mathbf{w}(\mathbf{x}, t) - \mathbf{u}) - g\mathbf{k}. \tag{4}$$

If $\mathbf{x}_{t_0}$ and $\mathbf{u}_{t_0}$ are estimates of the position and velocity of an ember at time t_0 then we compute in turn:

$$\mathbf{x}^* = \mathbf{x}_{t_0} + \mathbf{u}_{t_0} \frac{\delta t}{2}$$
$$\mathbf{u}^* = \mathbf{u}_{t_0} + \mathbf{a}(\mathbf{u}_{t_0}, \mathbf{x}_{t_0}, t_0) \frac{\delta t}{2}$$
$$\mathbf{x}_{t_0+\delta t} = \mathbf{x}_{t_0} + \mathbf{u}^* \delta t$$
$$\mathbf{u}_{t_0+\delta t} = \mathbf{u}_{t_0} + \mathbf{a}(\mathbf{u}^*, \mathbf{x}^*, t_0 + \delta t/2) \delta t.$$

A time step of $\delta t = 0.05$ s was used to integrate Eqs. (CTVA) and (VTVA), with $\delta t = 0.01$ s used for Eq. (NTVA). This choice of numerical method and time step is discussed further in Section 3.3. The initial conditions for Eqs. (CTVA) and (VTVA) are simply $\mathbf{x}(t_0) = \mathbf{x}_0$, where t_0 is the ember release time and $\mathbf{x}_0$ is the initial position of the ember (Section 2.3.2). The initial conditions for Eq. (NTVA) were taken to be $\mathbf{x}(t_0) = \mathbf{x}_0$, $\mathbf{u}(t_0) = \mathbf{w}(\mathbf{x}_0, t_0) - u_\infty \mathbf{k}$. Thus in all cases the ember is assumed to be initially travelling at approximately its terminal velocity (neglecting the factor ρ_0/ρ). In practice, because of the rapid approach to terminal velocity, the precise choice of initial velocity will have little overall effect on the results.

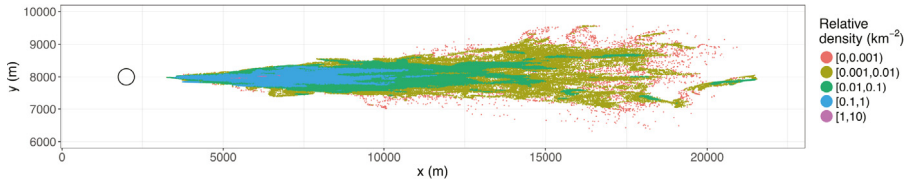

(a) Eqn. (CTVA): Constant terminal-velocity assumption

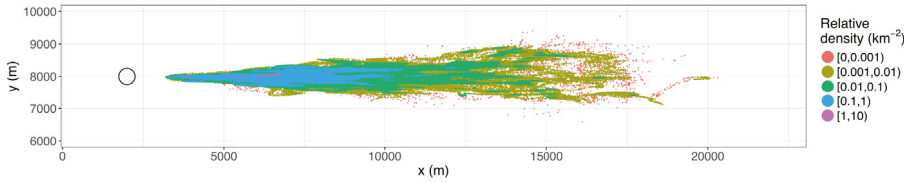

(b) Eqn. (VTVA): Variable terminal-velocity assumption

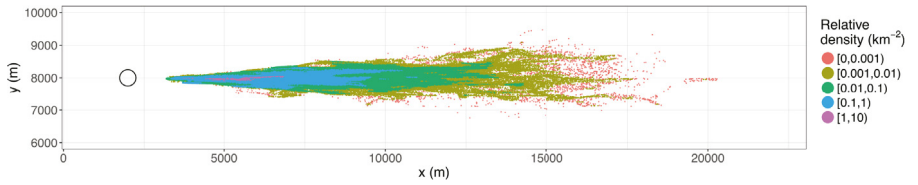

(c) Eqn. (NTVA) : No terminal-velocity assumption

Fig. 4. Location and density of ember landings for embers with $u_\infty = 6\ \mathrm{m\,s^{-1}}$ under: (a) the constant terminal-velocity assumption; (b) the variable-terminal-velocity assumption; and (c) no terminal-velocity assumption. Only embers that were transported at least 1 km under all three assumptions are included; 875,108 in total. Colours represent the density of landings per km^2 as a proportion of the total landings, computed using a Gaussian kernel density estimator. The circle shows the location and extent of the heat source used to generate the plume. Only part of the computational domain is shown.

3. Results and discussion

3.1. Results

Fig. 4 shows the two-dimensional landing distributions under the three transport assumptions for embers with $u_\infty = 6\ \mathrm{m\,s^{-1}}$. The points are coloured according to the density of landings at each location, estimated using a Gaussian kernel density estimator. Travel distances, and the density of embers travelling long distances, are clearly higher under the constant terminal-velocity assumption than those computed without any terminal-velocity assumption, with those computed using the variable terminal-velocity assumption assuming intermediate values.

Fig. 4 is difficult to interpret quantitatively so we focus now on travel distances rather than two-dimensional landing distributions. Fig. 5 shows the estimated probability distributions of travel distances for embers with $u_\infty = 3$, 6, and 8 $\mathrm{m\,s^{-1}}$ under the three transport assumptions (note that the horizontal scale differs in each panel). For $u_\infty = 6$ and 8 $\mathrm{m\,s^{-1}}$ (Fig. 5(b) and (c)), motion under the constant terminal-velocity assumption results in a significantly higher density of embers flying longer distances than when no terminal-velocity assumption is used (when interpreting Fig. 5 one should note the logarithmic scale on the vertical axis). For example, in Fig. 5(b), the density of embers travelling 15,000 m is approximately 14 times higher under the constant terminal-velocity assumption, and approximately 5 times higher under the variable terminal-velocity assumption, than it is if no terminal-velocity assumption is used. This is an important finding. In reality, not every ember that lands will ignite a spot fire; any modelling of spot-fire development will almost certainly be partly stochastic with the probability of ignition dependent on, among other things, ember landing densities. If this type of direct simulation of ember trajectories was used to model spot-fire development then these results indicate that the use of the constant terminal-velocity assumption would result in a significantly higher modelled probability of long-range spot-fire ignition. This is undesirable from a scientific point of view, and in an operational setting could result in sub-optimal choices for the allocation of suppression resources.

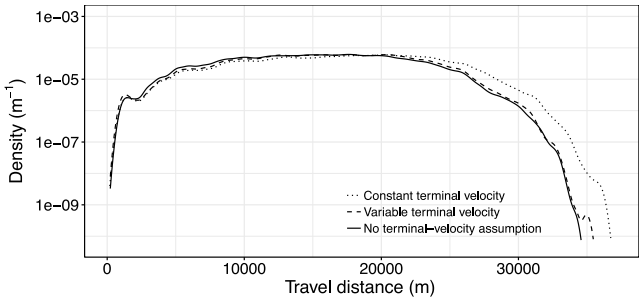

(a) $u_\infty = 3\ \mathrm{m\,s^{-1}}$.

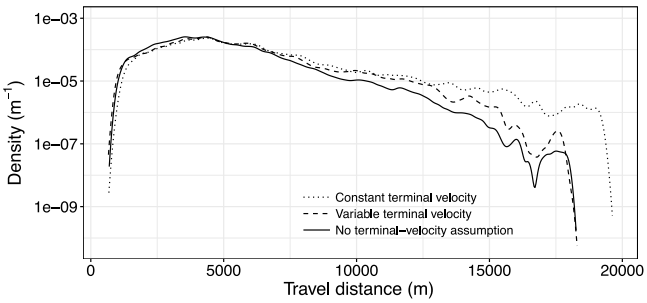

(b) $u_\infty = 6\ \mathrm{m\,s^{-1}}$.

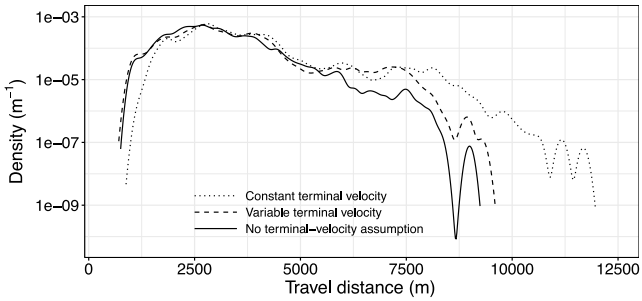

(c) $u_\infty = 8\ \mathrm{m\,s^{-1}}$.

Fig. 5. Gaussian kernel density estimates of the probability distributions of travel distances for embers with: (a) $u_\infty = 3\ \mathrm{m\,s^{-1}}$, (b) $u_\infty = 6\ \mathrm{m\,s^{-1}}$, and (c) $u_\infty = 8\ \mathrm{m\,s^{-1}}$. These can be converted into ember landing densities by multiplying by the number of embers. Only embers that have travelled further than 1 km under all three assumptions are included in the estimates. Note the scales on the x-axes differ.

How does the value of u_∞ affect the results? For small values of u_∞ the coefficient $1/{u_\infty}^2$ in Eq. (NTVA) is larger, so that the damping effect of the drag force is larger and the ember will approach its terminal velocity more quickly. Thus we expect smaller differences between motion under the variable terminal-velocity assumption and no terminal-velocity assumption. This is in agreement with Fig. 5(a) which shows distributions of travel distances when $u_\infty = 3\ \mathrm{m\,s^{-1}}$. There are still significant differences between motion under Eqs. (NTVA) and (CTVA); the latter neglects the effects of atmospheric density on the terminal fall speed.

3.2. Comparison with earlier study

In their study of short-range ember transport Koo et al. [6] found that using the terminal-velocity assumption underestimated ember transport distances and they attributed this to ‘the notion of a firebrand being thrown by locally strong winds’ when momentum is included in the equations of motion. This cannot be a major factor in the long-range transport of embers because an ember that has been ‘thrown’ will, within a few seconds, achieve terminal

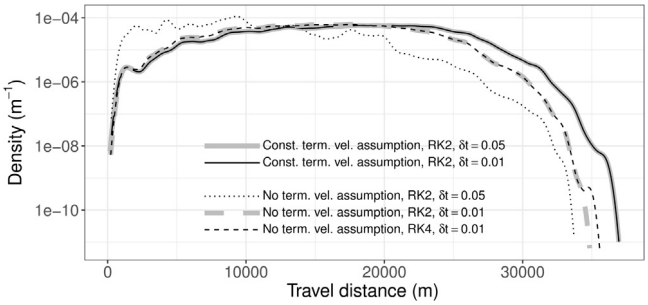

Fig. 6. Gaussian kernel density estimates of the probability distributions of travel distances using various time steps and numerical schemes for embers with $u_\infty = 3\ \mathrm{m\,s^{-1}}$.

velocity with respect to the wind field; embers cannot be thrown a long way. In our study embers are transported long distances because they are held aloft by the plume. When they leave the plume they fall to the ground, all the while being transported by the ambient wind. When modelled without the terminal-velocity assumption, embers have momentum and will not react instantaneously to changes in the turbulent wind field. This makes them more likely to leave the plume earlier, because they are more likely to either fall out if they do not respond quickly enough to an updraft that would keep them in the plume, or be thrown out by local turbulent motions.

3.3. Stability and accuracy of numerical scheme

The RK2 scheme (Section 2.3.3) was numerically unstable when attempting to integrate Eq. (NTVA) with $u_\infty = 2\ \mathrm{m\,s^{-1}}$ and $\delta t = 0.05$ s (results for $u_\infty = 2\ \mathrm{m\,s^{-1}}$ are not presented here). Eq. (NTVA) appears to be quite stiff, requiring very small time steps for smaller values of u_∞. We were able to integrate Eq. (NTVA) with $u_\infty = 2\ \mathrm{m\,s^{-1}}$ using RK2 with $\delta t = 0.01$ s, however this raises questions as to the accuracy of this scheme. To assess this we compared the results for Eq. (NTVA) integrated using RK2 with those obtained using the standard fourth-order Runge–Kutta scheme (RK4), which was implemented as follows: if $\mathbf{x}_{t_0}$ and $\mathbf{u}_{t_0}$ are estimates of the position and velocity of an ember at time t_0 then, with $\mathbf{a}(\mathbf{u}, \mathbf{x}, t)$ as defined by Eq. (4), we set $\mathbf{a}_0 = \mathbf{a}(\mathbf{u}_{t_0}, \mathbf{x}_{t_0}, t_0)$ and compute

$$\begin{aligned}
\mathbf{x}^* &= \mathbf{x}_{t_0} + \mathbf{u}_{t_0}\frac{\delta t}{2}, & \mathbf{u}^* &= \mathbf{u}_{t_0} + \mathbf{a}_0\frac{\delta t}{2}, & \mathbf{a}^* &= \mathbf{a}(\mathbf{u}^*, \mathbf{x}^*, t_0 + \frac{\delta t}{2}),\\
\mathbf{x}^{**} &= \mathbf{x}_{t_0} + \mathbf{u}^*\frac{\delta t}{2}, & \mathbf{u}^{**} &= \mathbf{u}_{t_0} + \mathbf{a}^*\frac{\delta t}{2}, & \mathbf{a}^{**} &= \mathbf{a}(\mathbf{u}^{**}, \mathbf{x}^{**}, t_0 + \frac{\delta t}{2}),\\
\mathbf{x}^{***} &= \mathbf{x}_{t_0} + \mathbf{u}^{**}\delta t, & \mathbf{u}^{***} &= \mathbf{u}_{t_0} + \mathbf{a}^{**}\delta t, & \mathbf{a}^{***} &= \mathbf{a}(\mathbf{u}^{***}, \mathbf{x}^{***}, t_0 + \delta t),
\end{aligned}$$

and finally

$$\begin{aligned}
\mathbf{x}_{t_0+\delta t} &= \mathbf{x}_{t_0} + \frac{1}{6}\left(\mathbf{u}_{t_0} + 2\mathbf{u}^* + 2\mathbf{u}^{**} + \mathbf{u}^{***}\right)\delta t,\\
\mathbf{u}_{t_0+\delta t} &= \mathbf{u}_{t_0} + \frac{1}{6}\left(\mathbf{a}_0 + 2\mathbf{a}^* + 2\mathbf{a}^{**} + \mathbf{a}^{***}\right)\delta t.
\end{aligned}$$

Results of the comparison for embers with $u_\infty = 3\ \mathrm{m\,s^{-1}}$ are depicted in Fig. 6. For Eq. (NTVA), there was good agreement between RK2 and RK4, using $\delta t = 0.01$ s. There is a slight difference at the tail of the distributions; this region contains few landing positions and the kernel density estimator is sensitive to slight differences in that region. RK2 with $\delta t = 0.05$ s is clearly not accurate.

Numerical stability is not at issue when integrating Eqs. (CTVA) and (VTVA). To assess the accuracy of the RK2 scheme for these equations, we compared results using $\delta t = 0.05$ and 0.01 s. Fig. 6 shows the results for Eq. (CTVA); they appear identical. A similar result was obtained for Eq. (VTVA) (not shown). In fact we could probably have used a larger value of δt with little loss of accuracy since, numerically, the right hand sides of Eqs. (CTVA) and (VTVA) are piecewise linear functions because they are interpolated linearly from the LEM data.

In this study the explicit, fixed time step Runge–Kutta schemes RK2 and RK4 were chosen primarily because of the ease with which they can be implemented. In a more comprehensive study, or in an operational setting, they may not prove to be the best choice, particularly for Eq. (NTVA) where an adaptive time step scheme or an implicit scheme might be more appropriate. Whatever numerical schemes are used, it is likely that ember trajectory calculations will be more computationally expensive if the terminal-velocity assumption is not made. This is certainly true for the RK2 scheme used in this study. Computational demand is not the focus of this paper although it will be an important consideration for large-scale modelling or in an operational setting.

4. Conclusion

In this study the validity of the terminal-velocity assumption was examined by simulating ember transport using data from a large eddy simulation of a turbulent plume. Two versions of the terminal-velocity assumption were studied: the constant terminal-velocity assumption, which neglects both ember momentum and variations in atmospheric density; and the variable terminal-velocity assumption, which neglects ember momentum but takes into account the atmospheric density at the location of the ember. We compared ember landing distributions computed under these assumptions with those computed using the equations of motion derived from the quadratic drag law, in which both ember momentum and atmospheric density are accounted for. Rotational motion of the embers was not considered, nor were the effects of in-flight combustion. We found that simulations using either version of the terminal-velocity assumption overestimated the density of long-range ember landings compared with simulations in which the terminal-velocity assumption is not made. This effect is greater for those embers with higher terminal fall speeds, and it is greater for the constant terminal-velocity assumption, which does not account for variations in atmospheric density. In our simulations embers were transported long distances because they were held aloft for long periods of time by the turbulent plume. If the terminal-velocity assumption is not used then the momentum of an ember increases the likelihood of it falling out of the plume, or being thrown out, because it does not react instantaneously to changes in the turbulent wind field; embers leave the plume earlier, and are not transported as far.

Although we did not include the effects of in-flight combustion on ember motion, it is likely that the results would be similar if these effects were considered. This is because changes to the flight characteristics of embers due to combustion occur on much longer time scales than the turbulent motion in the wind field. However further study needs to be done in order to characterise the effects of in-flight combustion and initial release heights on the observed landing distributions, particularly in light of the long flight times involved in long-range ember transport, and because initial release heights can affect flight times and therefore the potential for mass loss and aerodynamic changes.

Declaration of competing interest

The authors declare that they have no known competing financial interests or personal relationships that could have appeared to influence the work reported in this paper.

Acknowledgements

The authors would like to thank the anonymous reviewers for their helpful suggestions.

Funding

This research was supported by The Bushfire and Natural Hazards Cooperative Research Centre, and was undertaken with the assistance of resources and services provided by the National Computational Infrastructure (NCI), through the National Computational Merit Allocation Scheme, which is supported by the Australian Government.

References

[1] F.A. Albini, Spot Fire Distance from Burning Trees - a Predictive Model, General Technical Report INT-56, US Department of Agriculture Forest Service, Intermountain Forest and Range Experiment Station, Ogden, Utah, 1979.

[2] G.K. Batchelor, An Introduction to Fluid Dynamics, Cambridge University Press, 1967.

[3] J.L. Coen, M. Cameron, J. Michalakes, E.G. Patton, P.J. Riggan, K.M. Yedinak, WRF-fire: Coupled weather–wildland fire modeling with the weather research and forecasting model, J. Appl. Meteorol. Climatol. 52 (1) (2013) 16–38.

[4] P.F.M. Ellis, The effect of the aerodynamic behaviour of flakes of jarrah and karri bark on their potential as firebrands, J. R. Soc. West. Aust. 93 (2010) 21–27.
[5] K. Himoto, T. Tanaka, Transport of disk-shaped firebrands in a turbulent boundary layer, in: D.T. Gottuk, B.Y. Latimer (Eds.), Proceedings of the Eighth International Symposium on Fire Safety Science, International Association for Fire Safety Science, 2005.
[6] E. Koo, R.R. Linn, P.J. Pagni, C.B. Edminster, Modelling firebrand transport in wildfires using HIGRAD/FIRETEC, Int. J. Wildland Fire 21 (4) (2012) 396–417.
[7] C.-H. Moeng, P.P. Sullivan, A comparison of shear- and buoyancy-driven planetary boundary layer flows, J. Atmos. Sci. 51 (7) (1994) 999–1022.
[8] L.A. Oliveira, A.G. Lopes, B.R. Baliga, M. Almeida, D.X. Viegas, Numerical prediction of size, mass, temperature and trajectory of cylindrical wind-driven firebrands, Int. J. Wildland Fire 23 (5) (2014) 698–708.
[9] P.J. Richards, N. Williams, B. Laing, M. McCarty, M. Pond, Numerical calculation of the three-dimensional motion of wind-borne debris, J. Wind Eng. Ind. Aerodyn. 96 (10) (2008) 2188–2202.
[10] N. Sardoy, J.-L. Consalvi, B. Porterie, A.C. Fernandez-Pello, Modeling transport and combustion of firebrands from burning trees, Combust. Flame 150 (3) (2007) 151–169.
[11] W.C. Skamarock, J.B. Klemp, J. Dudhia, D.O. Gill, D.M. Barker, M. Duda, X.Y. Huang, W. Wang, J.G. Powers, A Description of the Advanced Research WRF Version 3, NCAR Technical Note NCAR/TN–475+STR, National Centre for Atmospheric Research, Boulder, Colorado, USA, 2008.
[12] M. Tachikawa, M. Fukuyama, Trajectories and velocities of typhoon-generated missiles, Trans. Archit. Inst. Japan 302 (1981) 1–11.
[13] C.S. Tarifa, P.P. del Notario, Open Fires and Transport of Firebrands, Technical Report, Instituto Nacional de Tecnica Aeronautica “Esteban Terradas”, Madrid, 1962.
[14] C.S. Tarifa, P.P. del Notario, F.G. Moreno, On the flight paths and lifetimes of burning particles of wood, in: Tenth Symposium (International) on Combustion, The Combustion Institute, 1965, pp. 1021–1037.
[15] C.S. Tarifa, P.P. del Notario, F.G. Moreno, A.R. Villa, Transport and Combustion of Firebrands, Technical Report, Instituto Nacional de Tecnica Aerospacial “Esteban Terradas”, Madrid, Spain, 1967.
[16] C.M. Thomas, J.J. Sharples, J.P. Evans, Evaluating the terminal-velocity assumption in simulations of long-range ember transport, in: G. Syme, D. Hatton MacDonald, B. Fulton, J. Piantadosi (Eds.), MODSIM2017, 22nd International Congress on Modelling and Simulation, The Modelling and Simulation Society of Australia and New Zealand Inc., Hobart, Tasmania, Australia, 2017, pp. 1187–1193.
[17] W. Thurston, J.D. Kepert, K.J. Tory, R.J.B. Fawcett, The contribution of turbulent plume dynamics to long-range spotting, Int. J. Wildland Fire 26 (4) (2017) 317–330.
[18] W. Thurston, K.J. Tory, R.J.B. Fawcett, J.D. Kepert, Large-eddy simulations of bushfire plumes in the turbulent atmospheric boundary layer, in: J. Piantadosi, R.S. Anderssen, J. Boland (Eds.), MODSIM2013, 20th International Congress on Modelling and Simulation, Modelling and Simulation Society of Australia and New Zealand, 2013, pp. 284–289.
[19] A. Tohidi, N.B. Kaye, Aerodynamic characterization of rod-like debris with application to firebrand transport, J. Wind Eng. Ind. Aerodyn. 168 (2017) 297–311.
[20] A. Tohidi, N.B. Kaye, Comprehensive wind tunnel experiments of lofting and downwind transport of non-combusting rod-like model firebrands during firebrand shower scenarios, Fire Saf. J. 90 (2017) 95–111.
[21] A. Tohidi, N.B. Kaye, Stochastic modeling of firebrand shower scenarios, Fire Saf. J. 91 (2017) 91–102.
[22] R. Wadhwani, D. Sutherland, A. Ooi, K. Moinuddin, G. Thorpe, Verification of a Lagrangian particle model for short-range firebrand transport, Fire Saf. J. 91 (2017) 776–783.